Journal of Theoretical Biology 333 (2013) 146–155

Contents lists available at SciVerse ScienceDirect

Journal of Theoretical Biology

journal homepage: www.elsevier.com/locate/yjtbi

Analysis of HRCT-derived xylem network reveals reverse flow in some vessels

Eric F. Lee [a,b,*], Mark A. Matthews [b], Andrew J. McElrone [b,c], Ronald J. Phillips [a], Kenneth A. Shackel [d], Craig R. Brodersen [e]

[a] Department of Chemical Engineering and Materials Science, One Shields Ave., University of California, Davis, CA 95616, USA
[b] Department of Viticulture and Enology, One Shields Ave., University of California, Davis, CA 95616, USA
[c] USDA-ARS, Crops Pathology and Genetics Research Unit, One Shields Ave., Davis, CA 95616, USA
[d] Department of Plant Science, University of California, One Shields Ave., Davis, CA 95616, USA
[e] Citrus Research & Education Center, University of Florida, 700 Experiment Station Rd., Lake Alfred, FL 33850, USA

HIGHLIGHTS

- Flow in some xylem vessels is found to be oriented in the opposite direction from the bulk.
- Reverse flow is seen in almost all simulations, indicating that it is a widespread phenomenon.
- Reverse flow is another mechanism for basipetal migration of *Xylella fastidiosa* in grapevine.
- The difference between *in planta* and *in vitro* migration rates of Xf is explained.

ARTICLE INFO

Article history:
Received 15 December 2012
Received in revised form
5 April 2013
Accepted 23 May 2013
Available online 4 June 2013

Keywords:
Computed tomography
Fluid mechanics
Modeling
Vitis vinifera
Xylella fastidiosa

ABSTRACT

Long distance water and nutrient transport in plants is dependent on the proper functioning of xylem networks, a series of interconnected pipe-like cells that are vulnerable to hydraulic dysfunction as a result of drought-induced embolism and/or xylem-dwelling pathogens. Here, flow in xylem vessels was modeled to determine the role of vessel connectivity by using three dimensional xylem networks derived from High Resolution Computed Tomography (HRCT) images of grapevine (*Vitis vinifera* cv. 'Chardonnay') stems. Flow in 4–27% of the vessel segments (i.e. any section of vessel elements between connection points associated with intervessel pits) was found to be oriented in the direction opposite to the bulk flow under normal transpiration conditions. In order for the flow in a segment to be in the reverse direction, specific requirements were determined for the location of connections, distribution of vessel endings, diameters of the connected vessels, and the conductivity of the connections. Increasing connectivity and decreasing vessel length yielded increasing numbers of reverse flow segments until a maximum value was reached, after which more interconnected networks and smaller average vessel lengths yielded a decrease in the number of reverse flow segments. Xylem vessel relays also encouraged the formation of reverse flow segments. Based on the calculated flow rates in the xylem network, the downward spread of *Xylella fastidiosa* bacteria in grape stems was modeled, and reverse flow was shown to be an additional mechanism for the movement of bacteria to the trunk of grapevine.

1. Introduction

Xylem conduits form a complex, interconnected network which distributes water between roots, leaves, and fruit in vascular plants. Under the extreme negative pressures maintained during transpiration, individual xylem conduits are prone to cavitation, the rapid phase change of liquid water to vapor (Tyree and Zimmermann, 2002). Possibly as a protection against the complete failure of the xylem network, vessels contain membranes with sub micrometer-sized pores that largely prevent gas flow between water-filled and gas-filled xylem conduits (Zimmermann and Brown, 1971; Tyree and Sperry, 1989; Choat et al., 2008). These membranes are located both in the lateral walls between neighboring conduits connected by pits and at the ends of xylem conduits. There exists a significant variation across species in the organization and distribution of the connections and vessel endings containing these membranes, with associated differences in

* Corresponding author at: 19600 Molalla Ave., Oregon City, OR 97045, USA. Tel.: +1 503 594 6163; fax: +1 503 650 6657.
E-mail addresses: elee@clackamas.edu (E.F. Lee), mamatthews@ucdavis.edu (M.A. Matthews), ajmcelrone@ucdavis.edu (A.J. McElrone), rjphillips@ucdavis.edu (R.J. Phillips), kashackel@ucdavis.edu (K.A. Shackel), brodersen@ufl.edu (C.R. Brodersen).

0022-5193/$ - see front matter © 2013 Elsevier Ltd. All rights reserved.
http://dx.doi.org/10.1016/j.jtbi.2013.05.021

the distribution of xylem conduit diameters (Pittermann, 2010). Conifer xylem networks are primarily comprised of tracheids with a fairly uniform size distribution, while angiosperm xylem networks are primarily comprised of vessels with a heterogeneous size distribution. It has been proposed that angiosperms have organized their networks with a heterogeneous distribution of vessel lengths and diameters so as to strike an evolutionary compromise between the efficiency of water transport and the safety against the failure of the network (e.g. Wheeler et al., 2005; Hacke et al., 2006).

The effects of the heterogeneous three-dimensional xylem structure on plant function have been primarily characterized through modeling efforts, due to the difficulty of taking measurements without disturbing the negative pressure environment. Sperry et al. (2005) quantified the effect of vessel length on vessel conductivity, defining a saturation length above which the plant's hydraulic conductivity remained nearly constant. They found that there was no advantage conferred to a plant that had vessels longer than the saturation length, as the network would become more vulnerable to embolisms without gaining any advantage in hydraulic conductivity. Loepfe et al. (2007) performed an extensive modeling study examining the role of the 3D structure of xylem and its function, generating networks by sampling from a series of biologically-based probability distributions for anatomical features and embolism spread. They did not explicitly report flow rates for individual vessels but showed in a figure a network with a heterogeneous set of flow rates. They proposed several organizational ideas based on the results of their model, including dead end segments, groups of isolated vessels, and segments with reverse flow. Some of these structures were not borne out by subsequent imaging studies (Brodersen et al., 2011). Their study was limited in that the geometry and connectivity of their generated networks were based entirely on sampling a series of normal distributions rather than analyzing structure based on an actual plant.

Significant advances in the understanding of the three-dimensional structure and connectivity of xylem in grape were made by Brodersen et al. (2011). They obtained anatomical data, network organizational structure, and connectivity by combining scanning electron microscopy for intervessel connection information, high resolution computed tomography (HRCT) for non-destructive network imaging, and custom software for the efficient analysis of the large amount of data associated with the HRCT scans. The results of their investigation revealed significantly heterogeneous xylem networks, with a distribution of vessel diameters, connection locations, and connection orientations. In addition, different parts of the cross-section of the stem showed variation, based on the sectoring of dorsal/ventral and lateral vessels as described by Stevenson et al. (2004).

In this study, we employed the methods developed in Brodersen et al. (2011) to translate HRCT scans into accurate virtual representations of xylem networks, which yielded precise information on the diameter, location, and orientation of vessels and their connections. Brodersen et al. (2013) found that xylem vessel relays, structures composed of a series of short, narrow diameter vessel elements that hydraulically connect neighboring vessels, are common in the two grape species examined (*Vitis vinifera* and *Vitis arizonica*). In *V. vinifera*, the pits connecting the vessel relay cells to the vessels all had either fully or partially degraded pit membranes, providing no protection against embolism or particulate (e.g. bacteria) movement between vessels. Because of the significant role that xylem vessel relays play in grapevine water transport, it was necessary to include these structures in the xylem networks for accurate transpiration modeling. We then modeled transpiration in the plant-based 3D networks, determining flow rates and pressure drops for individual vessels. Analyzing the relationship between network structure and flow patterns allowed us to determine how microstructural parameters influence the magnitudes and directions of local flow rates, with significant implications on both sap transport and bacterial spread. We then constructed a model xylem network using tubing, valves, and a pump to create a movie which demonstrates reverse flow with bubbles to aid in the visualization of the phenomena described in this manuscript.

2. Materials and methods

2.1. HRCT scans

A 2.7 cm length internode stem section of *V. vinifera* (cv. Chardonnay) was cut from a field grown plant and dried in an oven at 40 °C for 24 h to evacuate water from the vessel network. The section was then wrapped with Parafilm to prevent further dehydration. The section was then scanned at 15 keV in 0.125° increments over 180° at the x-ray micro-Tomography facility, Beamline 8.3.2 at the Advanced Light Source in Berkeley, California as described in Brodersen et al. (2011). Using Octopus Software (University of Ghent) the resulting series of 2D projection images were reconstructed into a 3D dataset, composed of virtual serial sections with a resolution of 4.5 μm. All data visualization was performed with Avizo 6.3 software (VSG, Inc., Burlington, Massachusetts, USA). Based on the 3D dataset, a set of modules in Avizo was used to construct a representation of the network of vessels and their connections as a series of segments (putative sections of vessels between connections) and network nodes (putative connections). Approximately 225 vessels were analyzed, divided into three different cropped sections of approximately 75 vessels each, with two sections from dorsal/ventral regions and 1 from a lateral region, using the anatomical sectoring terminology proposed by Stevenson et al. (2004).

2.2. Vessel endings

Vessel endings were not observed in the HRCT scans, and thus their frequency and distribution were measured using other experimental techniques. Complementary experimental data were obtained through resin casting and air and paint injection methods. For the resin casting, a 14.5 cm length section with a single node in the center from a current-year shoot of field grown *V. vinifera* cv. 'Chardonnay' was injected with a silicone elastomer (Rhodorsil RTV 141, Rhodia, Cranbury, NJ, USA) colored red with a pigment (LSDR-11, Dow Corning, Kendallville, IN, USA) (see (Sperry et al., 2005)). The stem section was connected to plastic tubing with one end submerged in a reservoir of elastomer inside a pressure chamber. Using an applied pressure of 0.15 MPa the elastomer was infiltrated for 30 min. The stem section was then oven dried at 70 °C overnight to cure the elastomer. Next, the wood surrounding the elastomer casts was dissolved with concentrated sulfuric acid and sodium hypochlorite following the methods of Kitin et al. (2001). The individual elastomer casts were then carefully separated and arranged on a glass plate where their lengths were measured with calipers. The resin casts did not provide an accurate distribution at the longer vessel lengths because the resin would often break during the extraction step. Nevertheless, the resin casts did provide detailed data for short vessel lengths, showing a uniform vessel length distribution for vessels with a length of 5 cm or less. To obtain the rest of the vessel length distribution, paint and air injection measurements were performed in the manner described in Chatelet et al. (2011), at intervals of ~3 cm. Similar results among the two injection methods were found. For a 2.7 cm long stem section, analysis of paint injection data indicated that 48% of the vessels would

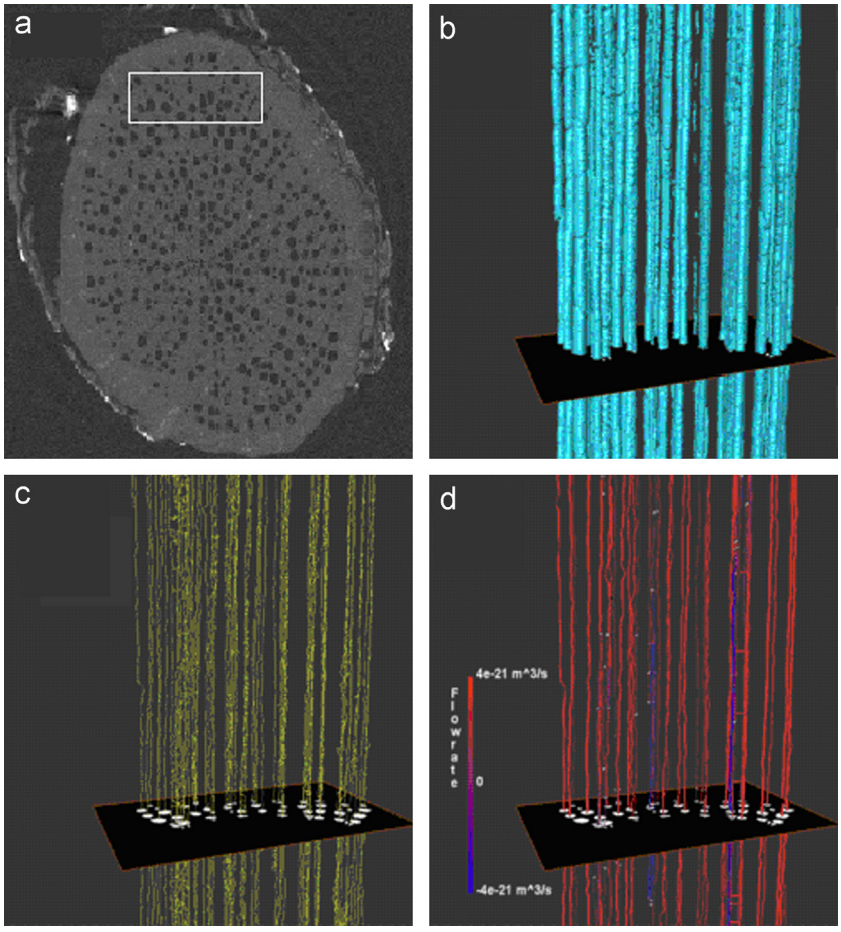

Fig. 1. A cross sectional image slice of a grapevine HRCT scan, with a white square that indicates that only part of the slice is examined in the later frames of the figure (a). A section of the slice, with a 3D surface representation of some xylem vessels (b). The blue represents the xylem vessels and the black represents the surrounding plant material. Avizo then calculates a preliminary series of network connections based on the HRCT-derived images (c). TANAX refines the network, and then flow simulations are performed to determine the flow rate in each vessel (d). The flow rates are color-coded based on their magnitude and direction, as indicated in the legend. Note that since the images are 2D graphical renderings of 3D structures, no scale bars are used since the scale is not consistent in different dimensions.

contain at least one ending somewhere in the stem section, and analysis of air injection data indicated that 61% of the vessels would contain at least one ending ((Chatelet et al., 2011), unpublished data from Eleanor Thorne). Vessel endings were modeled to be distributed randomly at the termini of vessel elements. Vessel elements, which are the building blocks of a vessel, were determined to have an average length of 750 μm through the length measurement of 50 vessel elements in Avizo (see Fig. 1(b)). Combining the average vessel element length with the average vessel ending percentage result from the two injection techniques (i.e. 55% of vessels have an ending) yielded that approximately 1.5% of all vessel elements contained a vessel ending.

2.3. Simulation of xylem flow

2.3.1. Xylem structure

An external program called Tomography-derived Automated Network Analysis of Xylem (TANAX) that was developed in FORTRAN (described in detail in (Brodersen et al., 2011)) eliminated the noise associated with the Avizo-generated network and used an experimentally determined separation distance threshold (14.0 μm) to specify intervessel connections. A few modifications of the TANAX software were made in order to incorporate short connecting xylem vessel relay elements, improve the accuracy of the intervessel connections, establish vessel endings, and efficiently perform network flow calculations.

The first new subroutine established xylem vessel relay elements, which are multicellular connecting elements between adjacent vessels that were recently discovered in grapevine (Brodersen et al., 2013). The algorithm used to define vessel relays was similar to the one used to define vessels. After eliminating the noise in the Avizo-generated network, all remaining segments that did not define the vessels were considered possible segments that might define vessel relay elements. Vessel relays were constructed acropetally, with successive segments selected based on their alignment with the vessels in the network, excluding dead-end and incorrectly oriented segments. Vessel relay elements with fewer than two connections to vessels or other vessel relays were eliminated, as these elements have no effect on network conductivity.

Two additional subroutines were developed in order to establish more accurate intervessel connections. Analysis of 8 SEM micrographs of intervessel pitfields showed that intervessel connections in grapevine have a minimum axial length of 56 μm; hence, intermittent and extremely short intervessel connections in the generated network were not permitted.

Intermittent connections were considered to be an artifact caused by noise in the HRCT scans. To account for this signal noise, in the first subroutine, missing intervessel connections were established. A connectivity parameter $c=(1-x/10)\times 10/9$ was defined, ranging in value from 0 to 1, where x is the number of slices out of a group of 10 slices that meet the connectivity threshold requirement of 14.1 μm for the closest voxels between neighboring vessels. A value of $c=0$ implied that every one of the

10 voxel slices met the threshold connection criterion for an intervessel connection to be established, while a value of $c=1$ implied that only one of the 10 voxel slices met the threshold criterion for an intervessel connection to be established. The second subroutine eliminated connections that were shorter than 56 μm.

Further modifications to the network were made by establishing vessel endings on 1.5% of all possible vessel elements, a percentage chosen based on the injection studies that gave the vessel length distribution. For each network segment, the number of possible vessel endings was determined by dividing the length of the segment by the average length of a vessel element. A random number was generated for each possible location of a vessel ending, and if the vessel ending probability was less than the generated number, a vessel ending was established at that location. The calculated number of possible vessel endings was not usually an integer, and thus the remaining fraction above the whole number was multiplied by the probability of vessel endings. If this number was less than the randomly generated number, an additional vessel ending was established.

2.3.2. Xylem flow

Calculations to determine the flow rate and pressure in individual vessels were performed using a second custom program that we developed in FORTRAN, called Interconnected Network FLow Of Water (INFLOW). In this program, the Hagen–Poiseuille law for fully developed, laminar flow in cylindrical tubes was solved for each network segment, and the conservation of mass equation was solved for each network node. The Hagen–Poiseuille approximation was warranted because the HRCT scans show that the xylem vessels are nearly cylindrical, and the vessel lengths are much greater than their radii. Since all of the resulting equations were coupled, they were solved simultaneously with matrix methods, yielding the flow rate in each network segment and the pressure at each network node. In order to improve computational performance, the system of equations was expressed in sparse matrix form and was then solved iteratively with the biconjugate gradient method for sparse matrices (Press et al., 1992).

Several additional parameters were required in order to perform flow calculations. A pit and vessel ending membrane resistance of 168 MPa s m^{-1} (Wheeler et al., 2005) and a vessel–vessel pit area fraction of 0.75 (Wheeler et al., 2005) were used. A water deficit of −2.0 MPa at the leaf of a typical *V. vinifera* shoot approximately 2 m long yields a pressure drop of −1.0 MPa per meter, and this pressure gradient was used to assign pressures at the bottom and top of the simulated networks. The qualitative results of the calculations are independent of the pressure drop because the system of equations is linear. In other words, if the pressure drop were doubled, then the flow rate in every vessel would double, but the number of reverse flow segments, the distribution of flow rates, and the ratio of the magnitudes of the flow rates would remain unchanged.

For networks in which conductive xylem vessel relays were included, an additional conductivity was needed to find the flow rate between vessels connected to vessel relays and/or interconnected vessel relay elements, based on the finding by Brodersen et al. (2013) that vessel relay pit membranes in *V. vinifera* are typically absent. The vessel–vessel relay and vessel relay-vessel relay pit conductivity was calculated by modeling the pits as rectangular prisms, with a pit aperture area A and a length L given by the intervessel distance, taken to be 14 μm. *V. vinifera* has scalariform pitting. The average dimensions of an individual pit aperture measure 50.8 μm by 2.3 μm and the average dimensions of the widest part of the pit measure 53.6 μm by 5.8 μm (Sun et al., 2006). Although there is some variation in pit dimensions in *V. vinifera*, we assume uniform pit geometry for simplicity. The pit resistance was determined by a geometric correction to the resistance based on a calculation for a circular pit. If the pits were circular in cross section, the area based resistance r'_B for a single pit would be given by

$$r'_B = \frac{\Delta P}{Q} A = \frac{32\ \mu L}{D^2}, \tag{1}$$

where P is the pressure, Q is the flow rate, and D is the diameter of the pit aperture. Since the individual pits are not circular in shape, we use an equivalent diameter D_e (equal to $4A/p$, where p is the perimeter of the pit aperture) in place of D (Wilkes, 1999) to find—

$$r'_B = \frac{32\ \mu L}{{D_e}^2} = \frac{2\ \mu L p^2}{A^2} = 23.1\ \frac{\text{kPa s}^{-1}}{\text{m}}. \tag{2}$$

Based on SEM images (Sun et al., 2006), within a pit field in grapevine there is approximately one pit every 6.7 μm. Combining this measurement with the measurement of the average pit aperture height (2.3 μm), we can estimate that 34% of the possible pitfield area is available for conduction. Hence the individual resistance is divided by 0.34 to give a pitfield resistance of $r_B = 67.9$ kPa s m^{-1}. As can be seen, the resistance of a pit without a membrane is over 1000 times smaller than that of a pit containing a membrane, yielding a dramatic change in the pathways that are most energetically favorable for sap transport.

For each simulation, 250 networks with differing vessel ending distributions were generated. Vessel endings were established based on a user-defined percentage of vessel elements with endings.

3. Results

A heterogeneous distribution of vessel diameters and intervessel connections was found in each xylem network (Fig. 1(a)). Using TANAX, the 3D rendering of the network (Fig. 1(b)) was converted into a ball and stick model (Fig. 1(c)), which included information on the vessel geometry and intervessel connections. INFLOW calculated the pressures at each network node and the flow rates in each segment. A few of the vessels (in blue) exhibited flow in the basipetal direction, while the majority of the vessels (in red) showed flow in the apical direction (Fig. 1(d)). Vessel relays, structures common in grapevine (Fig. 2(a)–(c)) were determined by TANAX and included in the INFLOW simulations, using appropriately modified pit resistances based on the lack of a membrane. The heterogeneous network gave rise to a wide range of flow rates (Fig. 3). Reverse flow was quantified by both the percentage of vessels and the longest contiguous set of segments with flow oriented in the basipetal direction.

Reverse flow was observed at a significantly higher frequency with the inclusion of vessel relays, and to a lesser degree with the inclusion of vessel endings. The frequency of reverse flow increased with increasing number of vessel endings until it reached a maximum at a vessel ending probability of approximately 0.1, where an average of 12% of the possible segments exhibited reverse flow (Fig. 4). While the results of Fig. 4 represent the average percentage of reverse flow segments for 250 networks with differing vessel ending distributions, the maximum percentage of segments with reverse flow observed for any one network was 27%. A higher vessel ending probability corresponds to a decrease in the average vessel length; hence the majority of the simulated results in Fig. 4 are for networks with average vessel lengths shorter than the value (0.015) for a 2.7 cm stem predicted by injection experiments. In other words, based on the experimental observations in grapevine, real networks have vessel ending probabilities less than 0.1. Thus while the theoretical results at very high vessel ending probabilities are of note, the general relationship between reverse

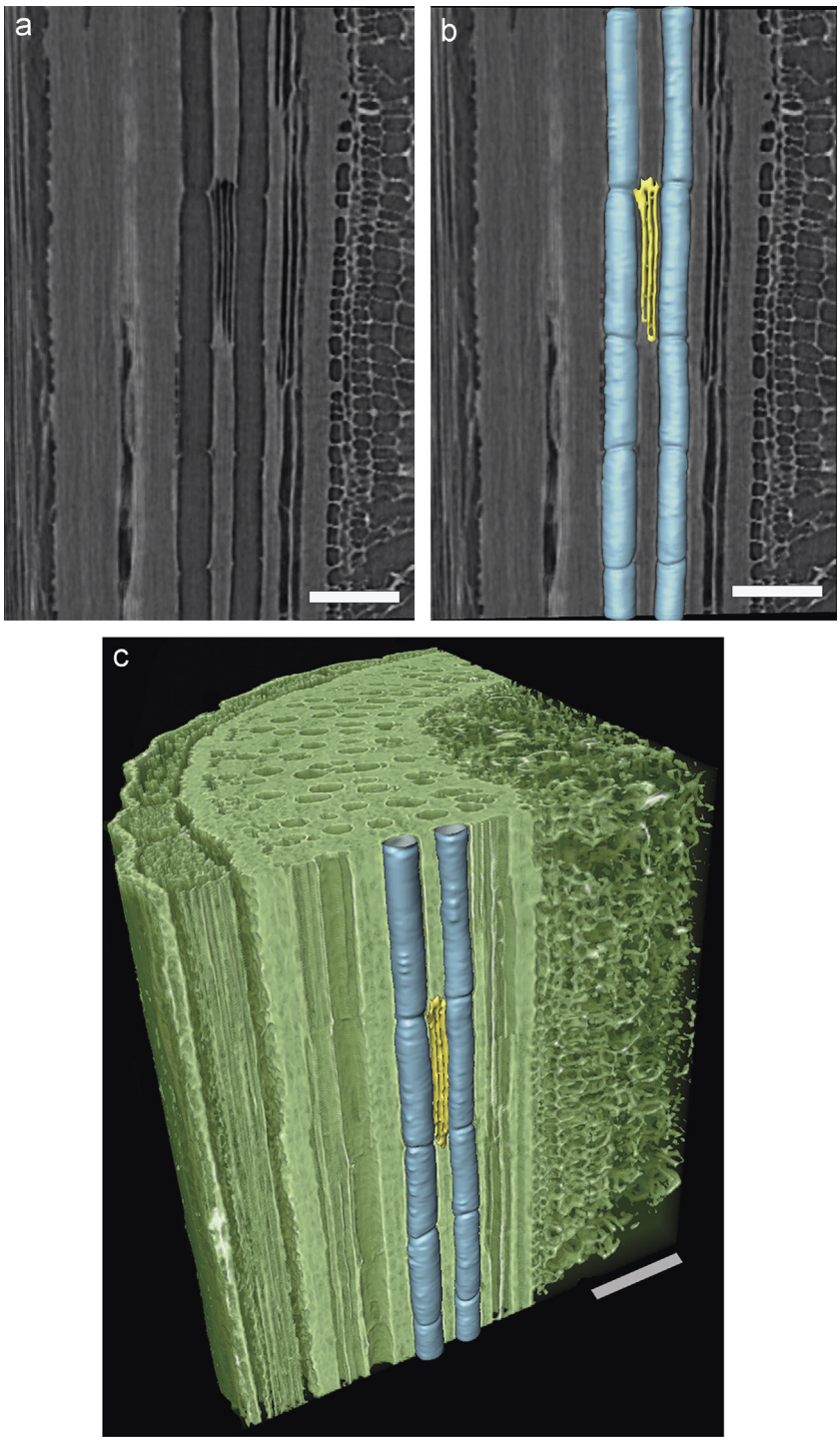

Fig. 2. Longitudinal HRCT images through *V. vinifera* xylem (a) and (b) showing a vessel relay (yellow, (b)) composed of three elements that connect two large diameter vessels (blue, (b)). In (c) the vessels connected by the relay are shown in their natural orientation within the stem. Bars=250 μm.

flow and vessel endings is that the incidence of reverse flow increases with the increased frequency of vessel endings for the biological realistic vessel ending probabilities less than 0.1.

The effect of vessel connectivity was next examined by varying the number of intervessel connections through the connectivity parameter. Networks with higher connectivity parameter values contained fewer reverse flow segments, with the exception of networks with $c=0.9$, which contained more reverse flow segments than networks with $c=0.7$ (see Fig. 4).

The inclusion of vessel relays led to a large increase in the number of segments exhibiting reverse flow. Fig. 5 shows a representative case ($c=0.5$), where the percentage of segments with reverse flow with the addition of vessel relays more than doubled for all values of vessel ending probability.

The longest contiguous reverse flow pathway was determined for each flow simulation by locating each reverse flow segment and then successively locating any reverse flow segments connected to the original segment, until reaching a point where the flow from all neighboring segments was acropetal. The algorithm included vessel relay connections but excluded intervessel connections, as only the vessel relay connections would serve as pathways for bacterial transport. The routine was repeated for

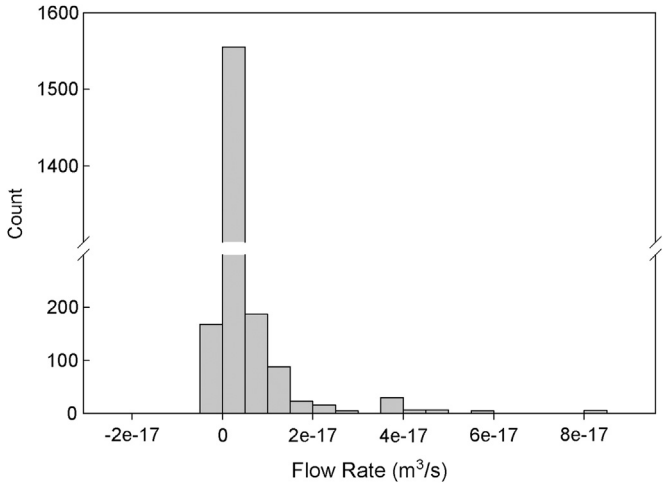

Fig. 3. Histogram of flow rates from a sample set of networks, including 2 D/V sectors and 1 lateral sector. Each count corresponds to one vessel segment with a flow rate in the corresponding bin. Each bin corresponds to 5×10^{-18} m^3 s^{-1}. The minimum and maximum flow speeds in this network are -2.11×10^{-17} m^3 s^{-1} and 8.69×10^{-17} m^3 s^{-1}, respectively.

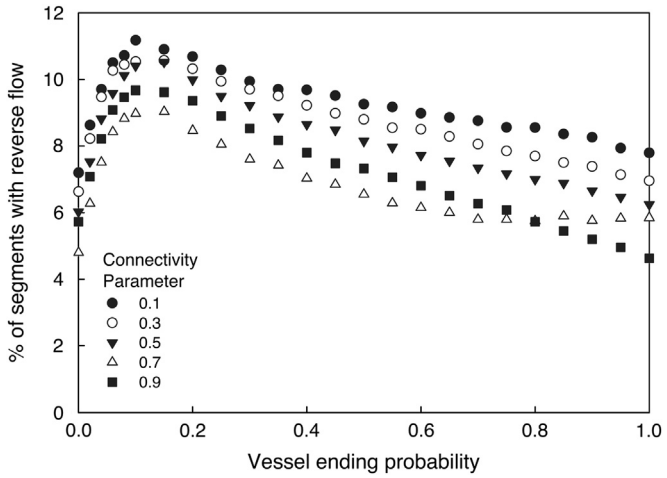

Fig. 4. Effect of connectivity on reverse flow. A connectivity parameter with a value of 0 indicates the most connected network, while a value of 1 indicates the least connected network. The connectivity parameter is related to the number of connections out of 10 possible connections that meet the threshold for the establishment of an intervessel connection as determined by SEM measurements. Each point represents 250 simulations, each with a different set of vessel ending locations established.

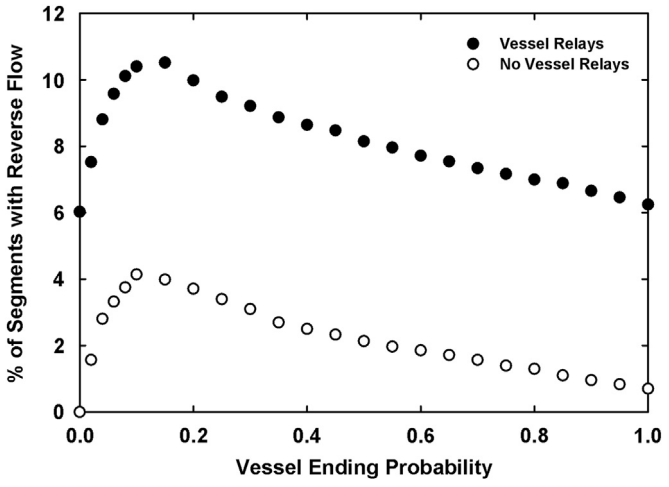

Fig. 5. Effect of vessel relays and vessel endings on percentage of reverse flow segments. Each point represents 250 simulations, each with a different set of vessel ending locations established. $c=0.5$.

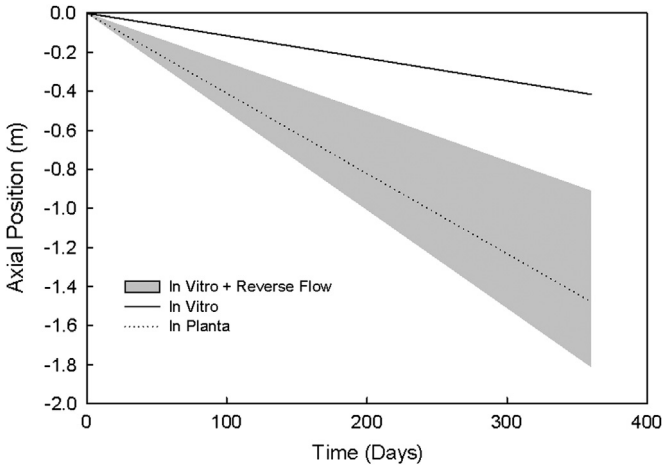

Fig. 6. Measurement of downward progress of *Xf* bacteria. *In vitro* migration position is based on the maximum observed speed noted in Meng et al. (2005). *In planta* measurements were also taken by Meng et al. (2005), with one data point obtained after bacterial movement was tracked for 11 weeks, with the initial distance traveled immediately following inoculation subtracted. *In vitro*+reverse flow shows the range of positions based on the speed of the bacteria plus the distance traveled by bacteria in reverse flow channels. For this case, vessel ending probabilities ranged from 0.5–3%, and c=0.5.

each reverse flow segment until the longest reverse flow pathway was determined.

The conceptual basis for the simulation of the *Xf* bacteria movement was the supplemental movies created by Hoch (⟨http://web.pppmb.cals.cornell.edu/hoch/movies/⟩), which show that some bacteria migrate preferentially against the transpiration current while others are swept with the current. In order to mimic the behavior seen in Hoch's movies, we assumed that the bacteria were carried in the direction of the current in basipetal, reverse flow segments and then migrated against the current in acropetal flow segments. This case is clearly does not apply for all bacteria, but we assume that there exist enough bacteria such that at least some always move in the basipetal direction. To find the maximum basipetal bacterial migration velocity, the length that the bacteria were required to swim against the current was determined by subtracting the length of the longest reverse flow pathway from the total stem length. In the vessels with acropetal flow, the bacteria were modeled to have the twitching migration velocity in the direction opposite to the bulk flow determined *in vitro* by Meng et al. (2005). The average bacterial migration velocity for the entire segment was then determined by combining the twitching migration against the current in vessels with acropetal flow with the migration with the current in vessels with basipetal flow.

The *in vitro* and *in planta* downward migration velocities reported in Meng et al. (2005) were compared with the predicted bacterial migration velocity for bacteria that both twitch to move in the direction opposite the bulk flow and utilize reverse flow pathways (Fig. 6). A range of simulations were performed, for vessel ending probabilities between 0.5% and 3.0%, and a connectivity parameter c of 0.5. A range of vessel ending probability parameters was included due to the uncertainty of the correct vessel length distribution. In general, simulations with fewer vessel endings yielded less reverse flow and, correlated with that, often a smaller basipetal migration distance. The resulting range of predicted bacterial velocities is shaded in gray and accounted for some, if not all, of the discrepancy between the *in vitro* and *in planta* rates of downward migration.

4. Discussion

We discovered a striking result in that individual vessels within the network display flow in the opposite direction to bulk flow. The usual assumption in applying the cohesion-tension theory is that the large scale bulk flow movement applies to the small scale as well, and hence each of the individual vessels and tracheids serves as a conduit for transport in the bulk direction (i.e. acropetally, from the roots toward the stem apex), with a more or less even distribution of sap flow velocities. We found, however, that this assumption does not always hold. In fact, the range of sap velocities is quite large, and the prevalence of reverse flow (i.e basipetal flow) in individual xylem vessels is high. Reverse flow occurred in most networks examined, suggesting that it is a phenomenon present in a number of network configurations.

More specifically, reverse flow occurred in every simulation in which vessel relays were included, regardless of the frequency of vessel endings or the intervessel connectivity present in the network. Reverse flow was also observed in simulations without vessel relays included, as long as the vessels contained at least some endings. To date, vessel relays have only been observed in grapevine (*V. vinifera* and *V. arizonica*) (Brodersen et al., 2013), although functionally analogous structures exist in other species (e.g. in palm, see (Fisher et al., 2002)). The observation of reverse flow in networks *without* vessel relays indicates that this phenomenon is likely widespread, occurring in many species.

Reverse flow conduits are found intermittently in the examined networks and form only when specific conductivity and connectivity requirements are met (see next section for more details). Reverse flow is not characterized by cyclical pathways but rather by short interruptions to acropetal movement via an intermediate vessel or vessel relay that connects two pathways with significantly different overall resistances. Connections to the intermediate segment must be oriented in such a way that basipetal flow is necessary for transport of the sap from the high to low resistance pathway. The sap in each reverse flow conduit eventually changes direction again, flowing through a pit to enter another conduit with acropetal flow. At this point, the sap resumes its rise toward the plant apex. It is important to note that sap that reverses direction is always moving in the energetically favored direction from a higher to a lower pressure. These pressure gradients arise from the heterogeneity in the xylem network.

Bulk reverse flow has been previously observed in a variety of situations (see e.g. Bleby et al., 2010; Windt et al., 2009; Burgess et al., 1998; Caldwell et al., 1998). Experimental studies have shown examples of bulk basipetal flow primarily occurring when the plant is redistributing water within its organs. Root systems redistribute water both acropetally (Caldwell et al., 1998) and basipetally (Bleby et al., 2010; Burgess et al., 1998; Gambetta et al., 2012) from soil at a higher water potential to soil at a lower water potential. A circulating flow (i.e. with both acropetal and basipetal direction flow components) has been observed in the trusses of tomato plants in the latter half of fruit development (Windt et al., 2009).

Despite widespread evidence and characterization of bulk reverse flow, to our knowledge a characterization of flow in individual vessels opposite in direction to the bulk flow has never been reported explicitly. One experimental study, however, gives direct evidence for reverse flow in individual conduits. Matsushima et al. (2009) developed a method to estimate water velocities in xylem networks with a D_20 tracer, finding that between 12% and 32% of the flow vectors pointed in the reverse direction, depending on the optical flow algorithm used. They ascribed these "false vectors" as errors in the method. The results from the present study suggest that the observed orientations of the vectors may have been correct.

Loepfe et al. (2007), in a modeling study, first proposed the possibility of reverse-direction flow in an individual vessel. Their study involved simulations which were based on applying a pressure gradient to a network formed by sampling from a series of normal distributions describing various network parameters. Their simulations showed that reverse flow would extend the path for water to travel from the roots to the shoots. They showed that this increase was inversely proportional to the average connectivity in the network. In the most extreme case, for the smallest value of the average connectivity, they found that the lumen pathway increased in length by 35%. The present study confirms the existence of reverse flow in an individual xylem conduit with data derived explicitly from plant stem sections. The demonstration of reverse flow in individual xylem vessels has far-reaching implications for the transport of any pathogen, fungus, or virus against the transpiration stream. It is also plausible that the transport of plant hormones in the xylem (e.g. abscisic acid) could be affected, which would in turn affect the "transpiration rate signal" (Hartung et al., 2002).

The reverse flow phenomenon is perhaps counter to expectation; if the primary role of the xylem is to transport water and dissolved nutrients from the roots to the leaves and reproductive organs, reverse flow in individual conduits is seemingly of no benefit to plant function. One possibility for the existence of reverse flow is that it is a necessary consequence of the built-in heterogeneity in the location and distribution of vessel diameters, vessel endings, and intervessel connections. It has been posited that a heterogeneous organizational structure is an evolutionary balance between safety and efficiency, where large diameter vessels provide pathways for efficient water transport while smaller, highly connected vessels provide safety against embolism spread when the plant is under severe water stress (Hacke et al., 2006).

4.1. Requirements for reverse flow and factors affecting its frequency of occurrence

Reverse flow only occurs for a specific distribution of vessel resistances and orientation of intervessel connections. At least three interconnected vessels are required; the first two vessels must contain a high resistance pathway above their connection (Fig. 7(a,i)). The position of the connection between the first and second vessels must be closer to the apex than the position of the connection between the second and third vessels (Fig. 7(a,ii)). Last, the third vessel must have a lower resistance to acropetal flow than the other two vessels (Fig. 7(a,iii), indicated by large diameter vessel without a vessel ending). Relaxing any of these requirements (see, e.g., Fig. 7(b) and (c)) yields a network that does not exhibit reverse flow. Movie S1 shows water flowing in a model network that mimicked the anatomical situation described above. Tubes and connectors represented vessel connections, and a pump was used to create a pressure gradient that induced flow. In the first part of the movie, valves on the left two tubes remain open, mimicking the situation in which neither tube has vessel endings. Next, the valves are closed, adding resistance to those pathways and inducing reverse flow. Then, each valve is partially opened to allow for flow through the valves, modeling a system with vessel endings. Lastly, the valves are opened fully and acropetal flow resumes.

The anatomical situation described above is more likely to occur whenever a vessel network is both sufficiently well connected and heterogeneous, with a distribution of intervessel connection locations, vessel ending locations, and vessel diameters (and hence distribution of conductivities). Vessels must be sufficiently connected so as to allow multiple pathways for water to flow, but they must not be so well connected that a surfeit of alternative low resistance pathways are available, and hence backflow through a connecting vessel would be unnecessary.

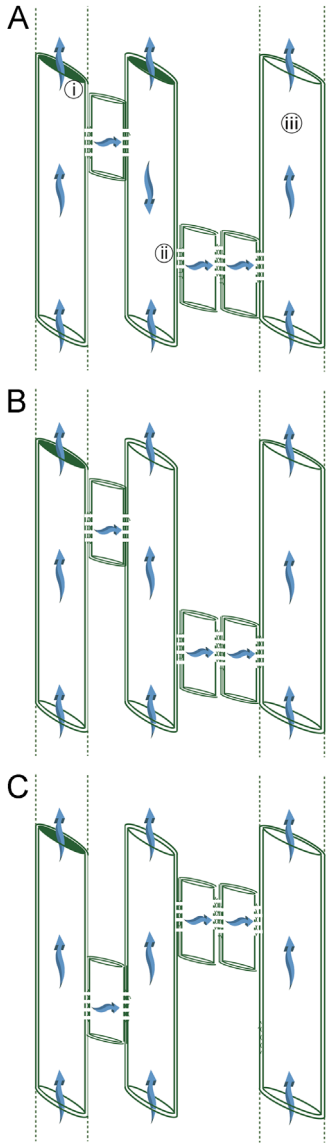

Fig. 7. Diagram depicting reverse flow (i). The left two vessels contain vessel endings (shaded), which increase the resistance in these pathways significantly (a). Flow from the leftmost vessel travels through a low resistance vessel relay and then flows basipetally (b). Flow then continues through a series of two vessel relays into a wide, highly conductive vessel (c). Two other diagrams show slight modifications in the xylem organization which would not yield reverse flow, because either the middle vessel lacked a vessel ending (ii) or the vessel relay connecting the second and third vessels were located at a position closer to the apex than the vessel relay connecting the first and second vessel (iii).

Grapevine xylem networks appear to have sufficient – but not excessive – connectivity so as to give rise to reverse flow segments. In terms of other aspects of heterogeneity in grapevine, experimental evidence suggests that a small percentage of vessel elements have endings. Grapevine vessels have a range of diameters, with the largest diameter vessels forming around halfway through the annual cycle, and the smaller diameter vessels in spring wood and late wood (Brodersen et al., 2011). Grapevine also displays sectoriality, with vessels in lateral sections having a smaller average diameter than in dorsal/ventral sections (Brodersen et al., 2011). Hence, grape wood is in all respects sufficiently heterogeneous to promote reverse flow.

Increased connectivity in the network is responsible for two competing effects. Additional intervessel connections give rise to new potential reverse flow pathways; simultaneously, however, they reduce the likelihood of reverse flow by reducing the heterogeneity in the network. Increased connectivity usually yields fewer reverse flow segments when connections between the same two vessels are repeated at different axial positions. On the other hand, the establishment of a connection between two previously unconnected vessels can lead to more reverse flow segments. This competition is illustrated in Fig. 4, where the most highly connected network (with $c=0.9$) has a higher frequency of reverse flow segments than the next most connected network (with $c=0.7$) when no vessel endings are established, largely because the most highly connected network featured many connections between previously unconnected vessels.

The percentage of vessels with reverse flow reaches a maximum at an intermediate vessel ending probability when the heterogeneity within the network is high. Increasing the vessel ending probability (in effect, decreasing the average vessel length) at low vessel ending probabilities yields an increase in the number of reverse flow segments until the number of reverse flow segments reaches a maximum when approximately 10% of the vessel elements have an ending. At higher vessel ending probabilities, the trend reverses as the heterogeneity in the network decreases. It is important to emphasize that experimental results indicate that the vessel ending probabilities are in the lower range, but the theoretical results at higher vessel ending probabilities are included for completeness.

The inclusion of vessel relays without pit membranes causes a large increase in the percentage of reverse flow segments (see Fig. 5). It is unsurprising that vessel relays have such a large effect on the percentage of vessels with reverse flow, based on the requirements for the creation of a reverse flow segment, coupled with the fact that vessel relays in *V. vinifera* have a very low resistance due to the lack of pit membranes between elements. Although not modeled in this study, vessel relays in *V. arizonica* contain intact membranes, and it would be expected that reverse flow would still occur in this species, albeit less frequently.

Since vessel relays have been observed thus far only in grapevine (Brodersen et al., 2013), reverse flow in other species is expected only when there is fairly high conductivity between vessels, possibly arising from changes in pit membrane conductivity based on enzymatic (Pérez-Donoso et al., 2010) or ionic (Zwieniecki et al., 2001) activity. Another scenario that would result in significant reverse flow – also present in grapevine – would be a sufficient frequency of vessel endings with resistances comparable or higher to those of pitfields.

4.2. Implications of reverse flow in bacteria spread

An important consequence of basipetal flow in certain vessels is the implication that it has on the basipetal spread of xylem-dwelling pathogens. We focus on the devastating *Xylella fastidiosa* (*Xf*) bacterium, which is transmitted by several sharpshooter species that feed on the xylem sap in grapevine. The sharpshooter inoculates the shoot with *Xf* bacteria while feeding, and the bacteria spread to other parts of the plant; if successful, the bacteria eventually infect the whole plant and cause Pierce's disease (Chatterjee et al., 2008). If, however, the bacteria do not reach the main trunk of the grapevine, springtime pruning eliminates the spread of the infection, and the overall plant remains healthy. Most sharpshooter species only feed on the new plant growth, and hence grapevines infected by these species develop long-term disease only from inoculations in the early spring, when bacteria have sufficient time to reach the main trunk before next year's pruning. The relatively recent introduction of the glassy-winged sharpshooter to California has exacerbated the spread of Pierce's disease, as this species of sharpshooter feeds on all parts of the grapevine cane, including the woodier parts near the trunk (Redak et al., 2004; Purcell and Feil 2001).

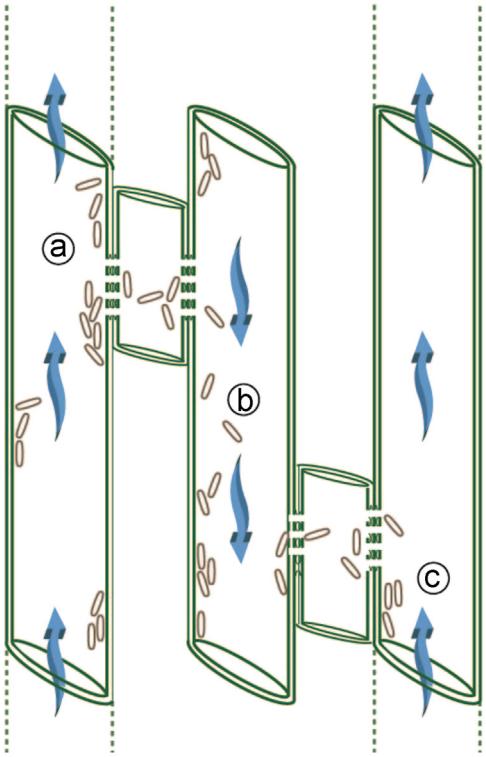

Fig. 8. Diagram of bacteria transport toward the basal part of the plant. Some bacteria swim against the transpiration stream (a). Then, some bacteria are carried in the direction of the current (b). Some bacteria then continue movement in the basipetal direction via continued movement against the current (c).

Thus, the principal requirement for the systemic infection of grapevine by *Xf* is bacterial movement in the basipetal direction. Meng et al. (2005) showed in several *in vitro* experiments that *Xf* bacteria were capable of moving opposite the direction of the bulk flow by employing a pilus-driven twitching mechanism. Their measurements showed that *Xf* bacteria were capable of swimming upstream *in vitro* at a maximum speed of approximately 70 $\mu m\ h^{-1}$ when present in a stream with a typical transpiration flow rate, and more slowly, with a maximum velocity of about 35 $\mu m\ h^{-1}$ and without directional preference when present in a stream under zero flow or non-transpiration conditions. Since significant transpiration flows only occur for half of the day, we can extrapolate to estimate the maximum annual bacterial spreading rate based on both of their measured *in vitro* bacterial twitching speeds to be approximately 0.0094 m $week^{-1}$.

In a separate experiment, Meng et al. (2005) inoculated a plant (*V. vinifera*) with *Xf* and then measured the amount of downward migration after 11 weeks, subtracting off the initial movement (determined in a separate experiment) which they attributed to cavitation of vessels upon inoculation. They found that the wild type bacteria migrated approximately 0.35 m over the course of 11 weeks, i.e. a migration rate of approximately 0.032 m $week^{-1}$.

Thus, basipetal migration speeds measured *in planta* were around three times faster than those measured *in vitro*, and hence the motility due to twitching is only a partial explanation for the bacterial basipetal migration observed *in planta*. Bacterial movement in the basipetal direction will be abetted by reverse flow segments in the xylem network (Fig. 6). In the best case scenario for the bacteria, first the bacteria swim against the flow and then enter a reverse flow channel, which aids their progress in movement toward the roots, until they swim against the current again (Fig. 8). In this manner, bacteria spread throughout the plant via a combination of passive and active transport mechanisms. Of course, most bacteria do not move in the basipetal direction at all times; for example, they might be swept up by the current when it would be beneficial to swim against the current. However, since there are numerous bacteria, at least some can be expected to move either with or against the current such that they always travel in the basipetal direction. By calculating the flow rate distribution on hundreds of model networks derived from HRCT scan data, we find a range of bacterial basipetal migration speeds that explains the gap between *in vitro* and *in planta* measurements.

A further explanation for downward migration could lie in the ability of bacteria to significantly alter the flow network by digesting pit membranes and vessel endings as shown by Pérez-Donoso et al. (2010). This digestion is necessary for the spread of *Xf*, as the bacteria are too large (≥250 nm × ≥1000 nm) to pass through the small pores (5–20 nm) of the pit membranes (Pérez-Donoso et al., 2010). In this manner, the bacteria create new low-resistance pathways (i.e. mimicking vessel relays). A cluster of bacteria near the new low-resistance pathway may also effectively act as a vessel ending by blocking flow, and thus increase the likelihood for the formation of a reverse flow segment in a neighboring connected vessel. Tyloses may also form in response to the bacterial infection (Sun et al., 2006), occluding the vessel and again encouraging neighboring reverse flow segments to form.

5. Funding source

National Science Foundation

The funding source had no role in the study design; collection, analysis, or interpretation of the data; or in the writing of the report or decision to submit the article for publication.

All authors participated in the research and article preparation.

Acknowledgments

The authors thank A. MacDowell, J. Nasiatka, and D. Parkinson of beamline 8.3.2 for their technical assistance, T. Knipfer for help with the creation of the supplemental movie demo, and J. Shogren for data analysis assistance. This research was funded by National Science Foundation Grant DBI—0818479 and USDA-ARS CRIS funding (Research Project #5306-21220-004-00). The Advanced Light Source is supported by the Director, Office of Science, Office of Basic Energy Sciences, of the U.S. Department of Energy under Contract No. DE-AC02-05CH11231. The TANAX and INFLOW source codes are available upon request.

References

Bleby, T.M., McElrone, A.J., Jackson, R.B., 2010. Water uptake and hydraulic redistribution across large woody root systems to 20 m depth. Plant Cell Environ. 33 (2), 2132–2148.

Brodersen, C., Lee, E., Choat, B., Jansen, S., Phillips, R., Shackel, K., McElrone, A., Matthews, M., 2011. Automated analysis of 3D xylem networks using high resolution computed tomography (HRCT). New Phytol. 191 (4), 1168–1179.

Brodersen, C., Choat, B., Chatelet, D., Shackel, K., Matthews, M., McElrone, A., 2013. Xylem vessel relays contribute to radial connectivity in grapevine stems (*Vitis vinifera* and *V. arizonica*; Vitaceae). Am. J. Bot. 100 (2), 314–321.

Burgess, S., Adams, M., Turner, N., King, C., 1998. The redistribution of soil water by tree root systems. Oecologia 115, 306–311.

Caldwell, M., Dawson, T., Richards, J., 1998. Hydraulic lift consequences of water efflux from the roots of plants. Oecologia 131, 151–161.

Chatelet, D., Wistrom, C., Purcell, A., Rost, T., Matthews, M., 2011. Xylem structure of four grape varieties and 12 alternative hosts to the xylem-limited bacterium *Xylella fastidiosa*. Ann. Botany 108 (1), 73–85.

Chatterjee, S., Almeida, R., Lindow, S., 2008. Living in two worlds: the plant and insect lifestyles of *Xylella fastidiosa*. Annu. Rev. Phytopathol. 46, 243–271.

Choat, B., Cobb, A., Jansen, S., 2008. Structure and function of bordered pits: new discoveries and impacts on whole-plant hydraulic function. New Phytol. 177, 608–626.

Fisher, J., Tan, H., Toh, L., 2002. Xylem of rattans: vessel dimensions in climbing palms. Am. J. Bot. 89, 196–202.
Gambetta, G., Manuck, C., Drucker, S., Shaghasi, T., Fort, K., Matthews, M.A., Walker, M.A., McElrone, A.J., 2012. The relationship between root hydraulics and scion vigour across Vitis rootstocks: what role do root aquaporins play? J. Exp. Bot. 63 (18), 6445–6455.
Hacke, U., Sperry, J., Wheeler, J., Castro, L., 2006. Scaling of angiosperm xylem structure with safety and efficiency. Tree Physiol. 26 (6), 689–701.
Hartung, W., Sauter, A., Hose, E., 2002. Abscisic acid in the xylem: where does it come from and where does it go? J. Exp. Bot. 53 (366), 27–32.
Kitin, P., Sano, Y., Funada, R., 2001. Analysis of cambium and differentiating vessel elements in Kalopanax pictus using resin cast replicas. IAWA J. 22 (1), 15–28.
Loepfe, L., Martinez-Vilalta, J., Piñol, J., Mencuccini, M., 2007. The relevance of xylem network structure for plant hydraulic efficiency and safety. J. Theor. Biol. 247, 788–803.
Matsushima, U., Herppich, W., Kardijilov, N., Graf, W., Nilger, A., Manke, I., 2009. Estimation of water flow velocity in small plants using cold neutron imaging with D20 tracer. Nucl. Instrum. Methods Phys. Res., Sect. A 605, 146–149.
Meng, Y., Li, Y., Galvani, C., Hao, G., Turner, J., Burr, T., Hoch, H., 2005. Upstream migration of *Xylella fastidiosa* via pilus-driven twitching motility. J. Bacteriol. 187, 5560–5567.
Pérez-Donoso, A., Sun, Q., Roper, M.C., Greve, L.C., Kirkpatrick, B., Labavitch, J., 2010. Cell wall-degrading enzymes enlarge the pore size of intervessel pit membranes in healthy and *Xylella fastidiosa*-infected grapevines. Plant Physiol. 152 (3), 1748–1759.
Pittermann, J., 2010. The evolution of water transport in plants: an integrated approach. Geobiology 8, 112–139.
⟨http://web.pppmb.cals.cornell.edu/hoch/movies/⟩ Last accessed: 12/11/12 Hoch Burr Lab, associated with research from [18].
Press, W., Teukolsky, S., Vettering, W., Flannery, B., 1992. Numerical Recipes in FORTRAN. Cambridge University Press, Cambridge.
Purcell A., Feil H. 2001. Glassy-winged sharpshooter. Pestic. Outlook.
Redak, R., Purcell, A., Blua, J., Mizzell, R., Andersen, P., 2004. The biology of xylem fluid-feeding insect *Xylella fastidiosa* and their relation to epidemiology. Annu. Rev. Entomol. 49, 243–270.
Sperry, J., Hacke, U., Wheeler, J., 2005. Comparative analysis of end wall resistivity in xylem conduits in xylem transport. Plant Cell Environ. 28, 456–465.
Stevenson, J., Matthews, M., Rost, T., 2004. Grapevine susceptibility to Pierce's disease I: Relevance of hydraulic architecture. Am. J. Enol. Vitic. 55, 228–237.
Sun, Q., Rost, T., Matthews, M., 2006. Pruning-induced tylose development in stems of current-year shoots of *Vitis vinifera* (Vitaceae). Am. J. Bot. 93, 1567–1576.
Tyree, M., Sperry, J., 1989. Vulnerability of xylem to cavitation and embolism. Annu. Rev. Plant Physiol. Plant Mol. Biol. 40, 19–38.
Tyree, M, Zimmermann, M., 2002. Xylem Structure and the Ascent of Sap. Springer-Verlag, New York.
Wheeler, J., Sperry, J., Hacke, U., Hoang, N., 2005. Inter-vessel pitting and cavitation in woody Rosacae and other vesselled plants: a basis for a safety versus efficiency trade-off in xylem transport. Plant Cell Environ. 28 (6), 800–812.
Wilkes, J.O., 1999. Fluid Mechanics for Chemical Engineers. Prentice Hall, Upper Saddle River, New Jersey.
Windt, C., Gerkema, E., Van As, H., 2009. Most water in the tomato truss is imported through the xylem, not the phloem: a nuclear magnetic resonance flow imaging study. Plant Physiol. 151, 830–842.
Zimmermann, M, Brown, C., 1971. Trees: Structure and Function. Springer-Verlag, New York.
Zwieniecki, M., Melcher, P., Holbrook, N.M., 2001. Hydrogel control of xylem hydraulic resistance in plants. Science 291, 1059–1062.